Research Article Vol. 32, No. 3 / 29 Jan 2024 / Optics Express 3308
Optics EXPRESS

Upconversion photoluminescence of monolayer WSe_2 with biaxial strain tuning

SHRAWAN ROY,[1] JIE GAO,[2,3] AND XIAODONG YANG[1,4]

[1]Department of Mechanical and Aerospace Engineering, Missouri University of Science and Technology, Rolla, MO 65409, USA
[2]Department of Mechanical Engineering, Stony Brook University, Stony Brook, NY 11794, USA
[3]jie.gao.5@stonybrook.edu
[4]yangxia@mst.edu

Abstract: Mechanical strain can be used to tune the optical properties of monolayer transition metal dichalcogenides (1L-TMDs). Here, upconversion photoluminescence (UPL) from 1L-WSe_2 flakes is tuned with biaxial strain induced by cruciform bending and indentation method. It is found that the peak position of UPL is redshifted by around 24 nm as the applied biaxial strain increases from 0% to 0.51%. At the same time, the UPL intensity increases exponentially for the upconversion energy difference that lies within a broad range between −157 meV to −37 meV. The observed linear and sublinear power dependence of UPL emission in 1L-WSe_2 with and without biaxial strain at three different excitation wavelengths of 784 nm, 800 nm, and 820 nm indicates the multiphonon-assisted one-photon upconversion emission process. The results of strain-dependent UPL emission from 1L-TMDs pave a unique path to the advances in photon upconversion applications and optoelectronic devices.

1. Introduction

Strain engineering is one of the most effective and broadly pursued technique that modulates the crystal lattice and electronic band structure of monolayer transition metal dichalcogenides (1L-TMDs) because of their strong resilient capacity towards the mechanical deformation [1–10]. Optical properties of TMDs such as Raman scattering, reflection, absorption, and photoluminescence (PL) can be tuned by strain not only in monolayer but also in multilayers [2–7]. Several approaches have been used to apply mechanical strain on TMDs, such as bending of TMDs flakes on flexible substrates [5,6], transferring them on patterned substrates [8,9], and forming wrinkles in TMDs [7,10]. 1L-TMDs are direct bandgap, tri-atomic layered semiconductor 2D materials with sub-nanometer thickness having characteristic tunable optoelectronic properties [11–15]. 1L-tungsten diselenide (1L-WSe_2) is one of the promising TMD materials with ambipolar nature, strong luminescence, and high-quality wafer-scale growth [16,17], which has been broadly used in the fields of valley-based electronics [18,19], optoelectronics and spintronics [20]. Upconversion photoluminescence (UPL) of 1L-TMDs is an exciting anti-Stokes photon emission process where the emitted photons have higher energy than the absorbed photons [21–26]. UPL phenomena have been broadly studied in different kinds of materials like organic dyes [27,28], quantum dots [29], quantum wells [30], and rare-earth-doped materials [31], which enable many applications in the fields of bioimaging [32,33], displays [34], optical refrigeration [35], photovoltaic energy conversion [36], and lasing emission [37]. The temperature tuning of phonon-assisted UPL in 1L-TMDs at elevated temperatures has been studied previously [25]. The strain tuning approach offers an alternative way to modulate the UPL process at room temperature. However, the strain tuning of UPL emission in 1L-TMDs has not been well demonstrated yet.

In this work, biaxial strain tuned UPL emission from mechanically exfoliated 1L-WSe_2 at room temperature is demonstrated, together with strain-dependent PL emission and Raman scattering. Biaxial tensile strain up to 0.51% is applied on 1L-WSe_2 transferred on flexible polycarbonate

#506243 https://doi.org/10.1364/OE.506243
Journal © 2024 Received 19 Sep 2023; revised 19 Nov 2023; accepted 21 Nov 2023; published 17 Jan 2024

Optics EXPRESS

(PC) cruciform substrate by using bending and indentation method. As the applied biaxial strain on 1L-WSe_2 increases from 0% to 0.51%, the UPL peak position is redshifted by around 24 nm with strain tuning gauge factor of 96 meV/% strain, while the UPL intensity grows exponentially at different excitation wavelengths of 784 nm, 800 nm, and 820 nm. Biaxial strain tuned UPL emission is observed within a broad range of the upconversion energy difference from −157 meV to −37 meV, along with two orders of magnitude enhancement of the integrated UPL emission intensity. The observed linear and sublinear power dependence of UPL emission at three different excitation wavelengths suggests that UPL emission in 1L-WSe_2 under biaxial strain is mediated by multiphonon absorption in one-photon regime. These results will open new opportunities in advancing future TMD-based tunable photon upconversion devices and applications in the emerging areas of night vision, infrared imaging, photodetection, and flexible optoelectronics.

2. 1L-WSe_2 sample preparation on PC cruciform substrate

1L-WSe_2 flakes are obtained by mechanical exfoliation method from a bulk WSe_2 crystal (2D Semiconductors) by the use of scotch tape. Thin layers of WSe_2 are separated from the bulk WSe_2 crystals by multiple exfoliation steps using scotch tape. Then the tape with WSe_2 thin flakes is gently placed on a small piece of polydimethylsiloxane (PDMS) film on a glass slide. After a while, the tape is gently removed from the PDMS film leaving multilayer and monolayer WSe_2 flakes on PDMS surface, and 1L-WSe_2 flakes are identified by the microscopic image, PL, and Raman characterizations. The cruciform is prepared from a 0.25 mm thick PC board, and the length and width of the cruciform is 60 mm and 8 mm, respectively [6]. Finally, the identified exfoliated 1L-WSe_2 flakes on PDMS are transferred to the PC cruciform substrate with the dry transfer technique [38], where an optical microscope integrated with a micromanipulator is used to precisely align the monolayers with the center of the PC substrate. Figure 1(a) shows the optical microscopic image of a WSe_2 flake transferred on PC cruciform, where 1L-WSe_2 region is marked by the white dotted lines. Biaxial tensile strain is applied to the 1L-WSe_2 on flexible PC cruciform substrate by cruciform bending and indentation method [6]. Figure 1(b) presents the schematic diagram of the biaxial strain tuning apparatus, where the biaxial strain is applied at the center area of the cruciform PC substrate clamped at its four edges. The sphere indenter under its geometrical center deflects the substrate upwards. This provides an equi-biaxial tensile strain applied on the top surface of the PC substrate. The biaxial strain level applied to the 1L-WSe_2 at the geometrical center of the PC cruciform is given by the equation $\varepsilon = 3Dt/L^2$, where L is the distance between the two opposing pivotal edges ($L = 25.4$ mm), t is the thickness of the cruciform PC substrate ($t = 0.25$ mm), and D is the deflection of the substrate at its center [6,39].

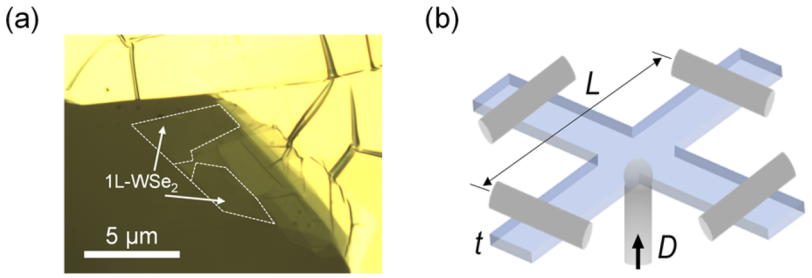

Fig. 1. (a) Optical microscope image of an exfoliated WSe_2 flake transferred on PC cruciform substrate, with 1L-WSe_2 region marked by the white dotted lines. (b) Schematic diagram of the biaxial strain apparatus, where biaxial strain applied on 1L-WSe_2 is induced by cruciform bending and indentation method.

Optics EXPRESS

3. Biaxial strain dependent UPL emission from 1L-WSe_2

The Raman spectra of 1L-WSe_2 flakes on flexible cruciform substrate are measured with a 633 nm He-Ne laser by collecting the back reflected signal through a 50X objective lens (NA = 0.42) coupled into a spectrometer (Horiba, iHR 550). The strain dependent Raman spectra of 1L-WSe_2 flakes are presented in Fig. 2(a). The representative Raman spectrum of 1L-WSe_2 at 0% strain (shown as the black curve) indicates the Raman peak position at ~ 250 cm^{-1} for the degenerated in-plane $E^1{}_{2g}$ and out-of-plane A_{1g} phonon vibrational modes. As the biaxial strain increases from 0% to 0.51%, the Raman peak position continuously redshifts by ~ 2.2 cm^{-1}, which is due to the strain induced crystal symmetry breaking and vibration softening [7,40]. Figure 2(b) shows the linear dependence of the Raman peak position on the applied strain, and a redshift of 4.31 cm^{-1}/% strain is obtained.

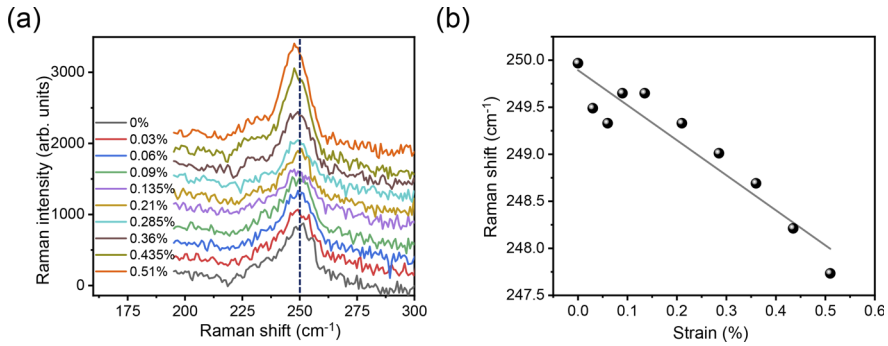

Fig. 2. (a) Strain dependent Raman spectra of 1L-WSe_2. (b) Variation of Raman shift as a function of the applied biaxial strain.

Figure 3 displays the biaxial strain dependent PL spectra excited at λ_{ex} = 633 nm and UPL spectra excited at λ_{ex} = 784 nm, 800 nm and 820 nm from 1L-WSe_2 on flexible cruciform substrate at room temperature. It is noted that the PL and UPL spectra are measured using the same experimental setup as the Raman characterization with different continuous-wave excitation lasers and the corresponding long pass or short pass filters. As shown in Fig. 3(a), the peak position of PL spectrum at 0% strain is located at 743 nm, which is consistent with the typical PL of 1L-WSe_2 [41,42]. The PL peak position exhibits a wavelength redshift as the applied biaxial strain increases gradually from 0% to 0.51%, while the PL intensity grows almost three times as the strain increases. As presented in Fig. 3(b-d), the UPL spectra of 1L-WSe_2 under 0% strain exhibit peak positions at around 742 nm under all three excitation wavelengths of 784 nm, 800 nm and 820 nm, which match with the measured PL peak position of 1L-WSe_2. When the biaxial strain level increases from 0% to 0.51%, the UPL peak positions are redshifted due to the reduced bandgap under strain, while the UPL emission intensity is significantly enhanced by 8, 7, and 6.5 times under the excitation of 784 nm, 800 nm, and 820 nm, respectively. In Fig. 3(b) and 3(c), the full range of UPL spectra is not provided due to the wavelength cutoff by a 775 nm short-pass filter.

Figure 4(a) further plots the PL and UPL peak positions depending on the applied biaxial strain under different excitation wavelengths, which clearly shows that the peak positions are redshifted as the biaxial strain increases, almost following a linear function of the strain level. It is found that the PL peak position redshift of ~ 23 nm is obtained at 0.51% biaxial strain compared to the case of 0% strain excited at 633 nm, and a linear slope of ~ 47 nm/% strain is presented due to the change in the bandgap under strain, which is similar to the previous works [6,43–45]. The UPL peak position redshifts are ~ 24 nm for all excitation wavelengths of 784 nm, 800 nm, and 820 nm when biaxial strain increases from 0% to 0.51%. The observed linear slopes of ~

Optics EXPRESS

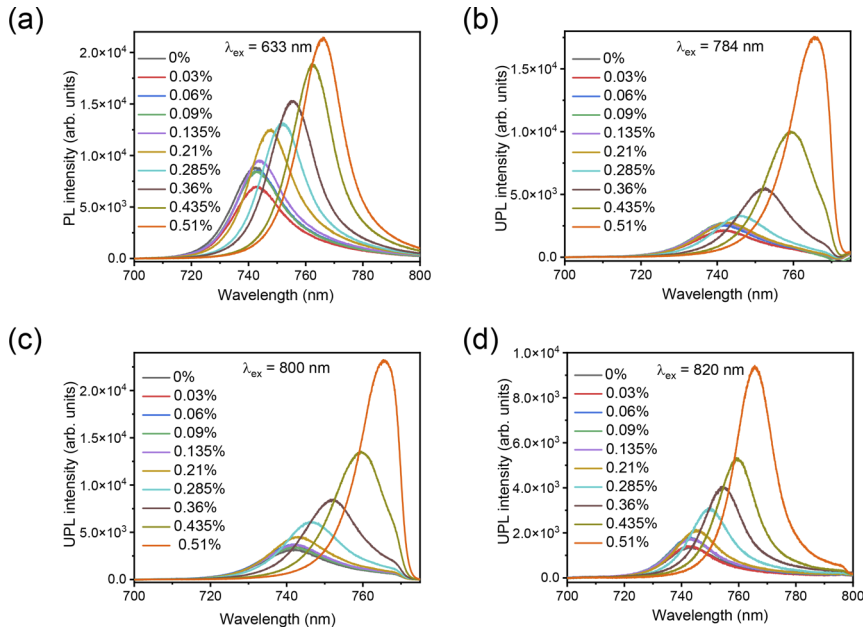

Fig. 3. (a) Strain dependent PL spectra from 1L-WSe_2 excited at 633 nm. (b)-(d) UPL spectra excited at 784 nm, 800 nm and 820 nm, respectively, for biaxial strain from 0% to 0.51%.

45 nm/% strain correspond to the UPL strain tuning gauge factor of 96 meV/% strain. The slight variation of the peak positions under different excitation wavelengths is induced by different strain transfer conditions between 1L-WSe_2 and cruciform substrate during each strain loading process. As the applied biaxial strain level on 1L-WSe_2 increases from 0% to 0.51%, the upconversion energy difference between the excitation photon energy and the UPL emission energy $\Delta E = \hbar\omega_{ex.}$-$\hbar\omega_{UPL}$ is continuously tuned under each excitation wavelength, with the value of −90 meV to −37 meV at the excitation wavelength of 784 nm, −122 meV to −69 meV at 800 nm, and −157 meV to −107 meV at 820 nm. Figure 4(b) plots the integrated UPL intensity as a function of the strain tuned ΔE ranging from −157 meV to −37 meV under three excitation wavelengths of 784 nm, 800 nm and 820 nm at room temperature. It is observed that the integrated UPL intensity exhibits an exponential growth with an enhancement in two orders of magnitude as ΔE is continuously tuned. The Boltzmann function can be used to describe the integrated UPL intensity as $I_{UPL} \propto \exp(-|\Delta E|/k_B T)$, with the upconversion energy gain $|\Delta E|$, the Boltzmann constant k_B, and the room temperature T of 298 K. The involved effective phonon number in the multiphonon-mediated upconversion photon emission process in 1L-WSe_2 can be approximately estimated from five to one according to the ratio between the strain tuned ΔE varying from −157 meV to −37 meV and the optical phonon energy of 31 meV for 1L-WSe_2. It is noteworthy that as the applied biaxial strain increases up to 0.51%, the variation of the optical phonon energy for 1L-WSe_2 is very small according to the measured strain dependent Raman shift shown in Fig. 2.

The representative power dependent PL and UPL spectra under 633 nm and 820 nm excitations with 0% and 0.48% applied strain are displayed in Fig. 5. As the excitation power increases, the spectral shapes and peak positions of both PL and UPL emission are maintained, while the emission intensities gradually grow as a function of the excitation power. Figures 6(a) and 6(b) present the power dependent integrated PL and UPL intensities from 1L-WSe_2 under the excitation wavelengths of 633 nm, 784 nm, 800 nm and 820 nm in a log-log scale at the biaxial strain levels of 0% and 0.48%, respectively. The PL and UPL intensities are fitted with the

Optics EXPRESS

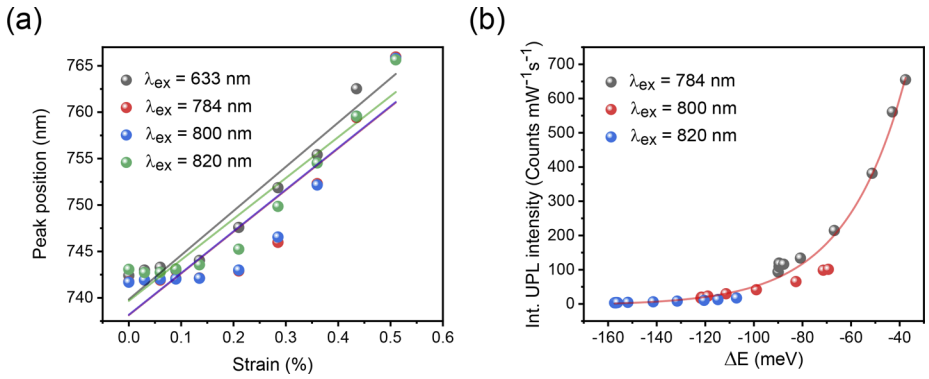

Fig. 4. (a) Dependence of PL and UPL peak positions on the applied biaxial strain for 1L-WSe_2 under different excitation wavelengths. (b) Integrated UPL intensity as a function of the upconversion energy difference ΔE obtained at different strain levels under three excitation wavelengths of 784 nm, 800 nm and 820 nm.

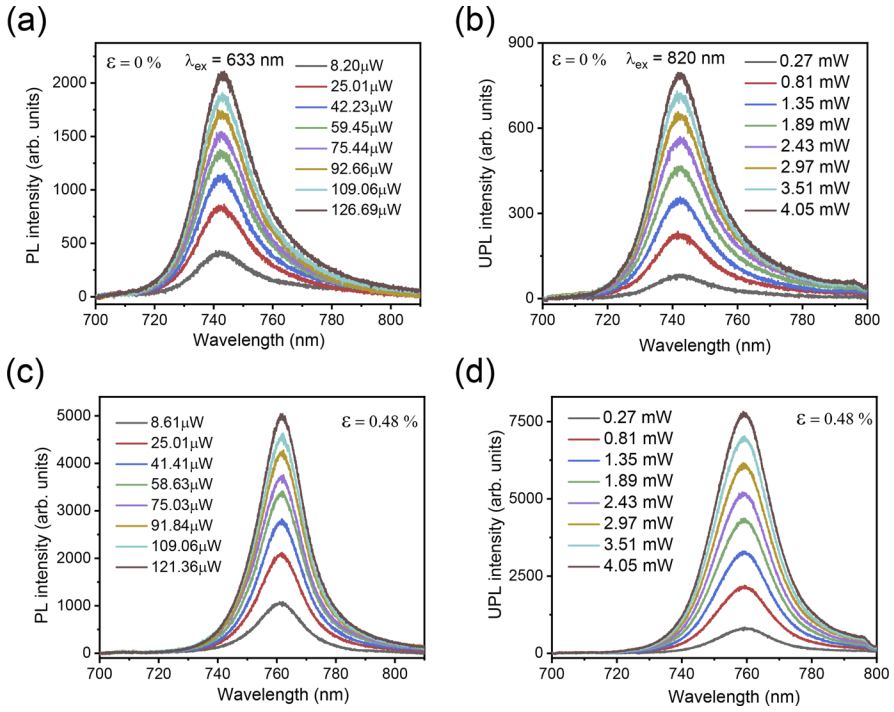

Fig. 5. Power dependent PL spectra under 633 nm excitation with (a) 0% and (c) 0.48% biaxial strain. Power dependent UPL spectra excited at 820 nm with (b) 0% and (d) 0.48% biaxial strain.

power law of $I = \alpha P^{\beta}$, with the excitation power P, the fitting parameter α, and the exponent β. At both biaxial strain levels, the fitted β values for the PL emission suggest a sublinear power dependence due to the strong quantum yield of 1L-WSe_2 and the saturated absorption at μW level excitation. For the UPL emission at both strain levels, the β value gets larger at a longer excitation wavelength, exhibiting a sublinear power dependence at the excitation wavelengths of 784 nm and 800 nm, and an almost linear power dependence at 820 nm. The sublinear power dependence

Optics EXPRESS

for the UPL emission may be related to the change of densities of phonons and exciton complexes [23]. The measured sublinear and linear power dependence of UPL emission from 1L-WSe_2 with biaxial strain indicates that the UPL emission follows a multiphonon-mediated one-photon upconversion process, which excludes other nonlinear effects such as two-photon absorption and Auger recombination.

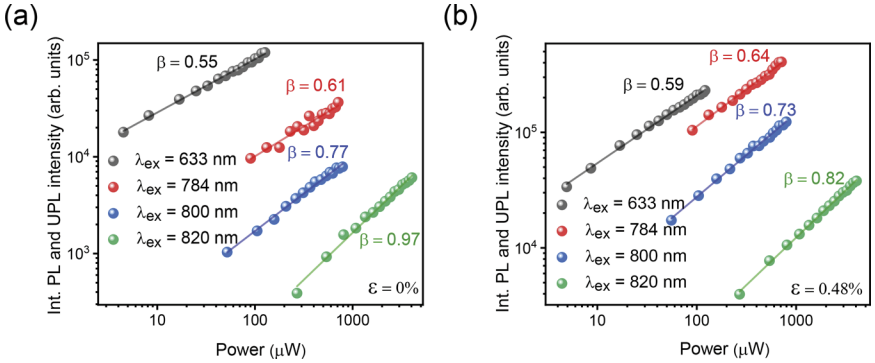

Fig. 6. Power dependent integrated PL and UPL intensities from 1L-WSe_2 in a log-log scale under the excitation wavelengths of 633 nm, 784 nm, 800 nm and 820 nm at the biaxial strain levels of (a) 0% and (b) 0.48%.

4. Conclusion

We have demonstrated biaxial strain tuned UPL emission in exfoliated 1L-WSe_2 on flexible cruciform substrate at room temperature by using bending and indentation method. The peak position of UPL emission is redshifted by around 24 nm as the applied biaxial strain on 1L-WSe_2 increases from 0% to 0.51% under different excitation wavelengths of 784 nm, 800 nm, and 820 nm, which corresponds to the UPL strain tuning gauge factor of 96 meV/% strain. It is shown that the UPL intensity grows exponentially as the strain increases, and two orders of magnitude enhancement of UPL intensity is achieved with the strain tuned upconversion energy difference varying from −157 meV to −37 meV. The measured linear and sublinear power dependence of UPL emission in 1L-WSe_2 with applied biaxial strain manifests that the UPL emission under strain tuning follows a multiphonon-mediated one-photon upconversion process. We believe that these results will pave the way to the advancement of strain tunable TMD-based light upconversion devices for future flexible photonics and optoelectronics.

Funding. Defense Advanced Research Projects Agency (W911NF2110353).

Acknowledgments. The authors acknowledge the support from the DARPA (W911NF2110353).

Disclosures. The authors declare no conflicts of interest.

Data availability. Data underlying the results presented in this paper are not publicly available at this time but may be obtained from the authors upon reasonable request.

References

1. R. Roldán, A. Castellanos-Gomez, E. Cappelluti, *et al.*, "Strain engineering in semiconducting two-dimensional crystals," J. Phys.: Condens. Matter **27**(31), 313201 (2015).
2. S. B. Desai, G. Seol, J. S. Kang, *et al.*, "Strain-induced indirect to direct bandgap transition in multilayer WSe_2," Nano Lett. **14**(8), 4592–4597 (2014).
3. W. Wu, J. Wang, P. Ercius, *et al.*, "Giant Mechano-Optoelectronic Effect in an Atomically Thin Semiconductor," Nano Lett. **18**(4), 2351–2357 (2018).
4. J. O. Island, A. Kuc, E. H. Diependaal, *et al.*, "Precise and reversible band gap tuning in single-layer $MoSe_2$ by uniaxial strain," Nanoscale **8**(5), 2589–2593 (2016).

Optics EXPRESS

5. F. Carrascoso, H. Li, R. Frisenda, *et al.*, "Strain engineering in single-, bi- and tri-layer MoS_2, $MoSe_2$, WS_2 and WSe_2," Nano Res. **14**(6), 1698–1703 (2021).
6. F. Carrascoso, R. Frisenda, and A. Castellanos-Gomez, "Biaxial versus uniaxial strain tuning of single-layer MoS_2," Nano Mater. Sci. **4**(1), 44–51 (2022).
7. K. P. Dhakal, S. Roy, H. Jang, *et al.*, "Local Strain Induced Band Gap Modulation and Photoluminescence Enhancement of Multilayer Transition Metal Dichalcogenides," Chem. Mater. **29**(12), 5124–5133 (2017).
8. H. Li, A. W. Contryman, X. Qian, *et al.*, "Optoelectronic crystal of artificial atoms in strain-textured molybdenum disulphide," Nat. Commun. **6**(1), 7381 (2015).
9. J. Chaste, A. Missaoui, S. Huang, *et al.*, "Intrinsic Properties of Suspended MoS_2 on SiO_2/Si Pillar Arrays for Nanomechanics and Optics," ACS Nano **12**(4), 3235–3242 (2018).
10. J. Wang, M. Han, Q. Wang, *et al.*, "Strained Epitaxy of Monolayer Transition Metal Dichalcogenides for Wrinkle Arrays," ACS Nano **15**(4), 6633–6644 (2021).
11. S. Roy, W. Choi, S. Jeon, *et al.*, "Atomic Observation of Filling Vacancies in Monolayer Transition Metal Sulfides by Chemically Sourced Sulfur Atoms," Nano Lett. **18**(7), 4523–4530 (2018).
12. S. Roy, G. P. Neupane, K. P. Dhakal, *et al.*, "Observation of Charge Transfer in Heterostructures Composed of $MoSe_2$ Quantum Dots and a Monolayer of MoS_2 or WSe_2," J. Phys. Chem. C **121**(3), 1997–2004 (2017).
13. K. P. Dhakal, S. Roy, S. J. Yun, *et al.*, "Heterogeneous modulation of exciton emission in triangular WS_2 monolayers by chemical treatment," J. Mater. Chem. C **5**(27), 6820–6827 (2017).
14. M. S. Kim, S. Roy, J. Lee, *et al.*, "Enhanced Light Emission from Monolayer Semiconductors by Forming Heterostructures with ZnO Thin Films," ACS Appl. Mater. Interfaces **8**(42), 28809–28815 (2016).
15. S. Roy, M.-H. Doan, J. Kim, *et al.*, "Modulation of optoelectric properties of monolayer transition metal dichalcogenides placed on a metal pattern," J. Korean Phys. Soc. **78**(8), 693–699 (2021).
16. J.-K. Huang, J. Pu, C.-L. Hsu, *et al.*, "Large-Area Synthesis of Highly Crystalline WSe_2 Mono layers and Device Applications," ACS Nano **8**(1), 923–930 (2014).
17. Z. Wang, Q. Li, Y. Chen, *et al.*, "The ambipolar transport behavior of WSe_2 transistors and its analogue circuits," NPG Asia Mater. **10**(8), 703–712 (2018).
18. K. Hao, G. Moody, F. Wu, *et al.*, "Direct measurement of exciton valley coherence in monolayer WSe_2," Nat. Phys. **12**(7), 677–682 (2016).
19. Z. Wang, J. Shan, and K. F. Mak, "Valley- and spin-polarized Landau levels in monolayer WSe_2," Nat. Nanotechnol. **12**(2), 144–149 (2017).
20. C. Robert, S. Park, F. Cadiz, *et al.*, "Spin/valley pumping of resident electrons in WSe_2 and WS_2 monolayers," Nat. Commun. **12**(1), 5455 (2021).
21. A. M. Jones, H. Yu, J. R. Schaibley, *et al.*, "Excitonic luminescence upconversion in a two-dimensional semiconductor," Nat. Phys. **12**(4), 323–327 (2016).
22. M. Manca, M. M. Glazov, C. Robert, *et al.*, "Enabling valley selective exciton scattering in monolayer WSe_2 through upconversion," Nat. Commun. **8**(1), 14927 (2017).
23. J. Jadczak, L. Bryja, J. Kutrowska-Girzycka, *et al.*, "Room temperature multi-phonon upconversion photoluminescence in monolayer semiconductor WS_2," Nat. Commun. **10**(1), 107 (2019).
24. A. Mushtaq, X. Yang, and J. Gao, "Unveiling room temperature upconversion photoluminescence in monolayer WSe_2," Opt. Express **30**(25), 45212 (2022).
25. F. Meng, X. Yang, and J. Gao, "Phonon-assisted upconversion photoluminescence of monolayer MoS_2 at elevated temperature," Opt. Express **31**(17), 28437 (2023).
26. F. Meng, X. Yang, and J. Gao, "High-temoerature phonon-assisted upconversion photoluminescence of monolayer WSe_2 at elevated temperature," Appl. Phys. Lett. **123**(1), 013502 (2023).
27. J. Zhao, S. Ji, and H. Guo, "Triplet–triplet annihilation based upconversion: from triplet sensitizers and triplet acceptors to upconversion quantum yields," RSC Adv. **1**(6), 937 (2011).
28. S. Baluschev, T. Miteva, V. Yakutkin, *et al.*, "Up-conversion fluorescence: noncoherent excitation by sunlight," Phys. Rev. Lett. **97**(14), 143903 (2006).
29. Z. Deutsch, L. Neeman, and D. Oron, "Luminescence upconversion in colloidal double quantum dots," Nat. Nanotechnol. **8**(9), 649–653 (2013).
30. G. Bacher, C. Hartmann, H. Schweizer, *et al.*, "Exciton dynamics in InxGa1−xAs/GaAs quantum-well heterostructures: Competition between capture and thermal emission," Phys. Rev. B **47**(15), 9545–9555 (1993).
31. F. Auzel, "Upconversion and anti-Stokes processes with f and d ions in solids," Chem. Rev. **104**(1), 139–174 (2004).
32. C. Vinegoni, D. Razansky, S. A. Hilderbrand, *et al.*, "Transillumination fluorescence imaging in mice using biocompatible upconverting nanoparticles," Opt. Lett. **34**(17), 2566 (2009).
33. C. T. Xu, N. Svensson, J. Axelsson, *et al.*, "Autofluorescence insensitive imaging using upconverting nanocrystals in scattering media," Appl. Phys. Lett. **93**(17), 171103 (2008).
34. E. Downing, L. Hesselink, J. Ralston, *et al.*, "A Three-Color, Solid-State, Three-Dimensional Display," Science **273**(5279), 1185 (1996).
35. R. I. Epstein, M. I. Buchwald, B. C. Edwards, *et al.*, "Observation of laser-induced fluorescent cooling of a solid," Nature **377**(6549), 500 (1995).
36. V. Gray, D. Dzebo, M. Abrahamsson, *et al.*, "Triplet–triplet annihilation photon-upconversion: towards solar energy applications," Phys. Chem. Chem. Phys. **16**(22), 10345–10352 (2014).

Optics EXPRESS

37. G. S. He, P. P. Markowicz, T.-C. Lin, *et al.*, "Observation of stimulated emission by direct three-photon excitation," Nature **415**(6873), 767 (2002).
38. Q. Zhao, T. Wang, Y. K. Ryu, *et al.*, "An inexpensive system for the deterministic transfer of 2D materials," JPhys Mater. **3**(1), 016001 (2020).
39. C. Androulidakis, E. N. Koukaras, J. Parthenios, *et al.*, "Graphene flakes under controlled biaxial deformation," Sci. Rep. **5**(1), 18219 (2015).
40. A. Castellanos-Gomez, R. Roldan, E. Cappelluti, *et al.*, "Local strain engineering in atomically thin MoS_2," Nano Lett. **13**(11), 5361–5366 (2013).
41. X. Chen, Z. Wang, L. Wang, *et al.*, "Investigating the dynamics of excitons in monolayer WSe_2 before and after super acid treatment," Nanoscale **10**(19), 9346–9352 (2018).
42. N. Mondal, N. Azam, Y. N. Gartstein, *et al.*, "Photoexcitation dynamics and long-lived excitons in strain-engineered transition metal dichalcogenides," Adv. Mater. **34**(23), 2110568 (2022).
43. B. Aslan, M. Deng, and T. F. Heinz, "Strained bilayer WSe_2 with reduced exciton-phonon coupling," Phys. Rev. B **98**(11), 115308 (2018).
44. C. Wang, Y. Wang, X. Su, *et al.*, "Extrinsic green photoluminescence from the edges of 2D cesium lead halides," Adv. Mater. **31**(33), 1902492 (2019).
45. S. Dai, X. Xing, V. G. Hajdiev, *et al.*, "Theory and experiments of pressure-tunable broadband light emission from self-trapped excitons in metal halide crystals," Mater. Today Phys. **30**, 100926 (2023).